

# Epitaxial Growth of Large Area Single-Crystalline Few-Layer MoS<sub>2</sub> with Room Temperature Mobility of 192 cm<sup>2</sup>V<sup>-1</sup>S<sup>-1</sup>

*Lu Ma<sup>1</sup>, Digbijoy N. Nath<sup>2</sup>, Edwin W. Lee II<sup>2</sup>, Choong Hee Lee<sup>2</sup>, Aaron Arehart<sup>2</sup>, Siddharth Rajan<sup>2\*</sup>, Yiying Wu<sup>1\*</sup>*

<sup>1</sup>Department of Chemistry & Biochemistry, The Ohio State University, 100 West 18<sup>th</sup> Avenue, Columbus, Ohio 43210.

<sup>2</sup>Department of Electrical and Computer Engineering, The Ohio State University, Columbus, Ohio 43210.

## AUTHOR INFORMATION

### Corresponding Author

\* Author to whom correspondence should be addressed. (Y.W.) Phone: (+1) 614-247-7810, Fax: (+1) 614-292-1685, Email: [wu@chemistry.ohio-state.edu](mailto:wu@chemistry.ohio-state.edu); (S.R.) Phone: (+1) 614-247-7922, Fax: (+1) 614-247-7596, Email: [rajan.21@osu.edu](mailto:rajan.21@osu.edu).

## KEYWORDS

molybdenum disulfide; vapor-solid growth; Van der Waals epitaxy; mobility; transition metal dichalcogenides;

## ABSTRACT

We report on the vapor-solid growth of single crystalline few-layer MoS<sub>2</sub> films on (0001)-oriented sapphire with excellent structural and electrical properties over centimeter length scale. High-resolution X-ray diffraction scans indicated that the films had good out-of-plane ordering and epitaxial registry. A carrier density of  $\sim 2 \times 10^{11} \text{ cm}^{-2}$  and a room temperature mobility of 192 cm<sup>2</sup>/Vs were extracted from space-charge limited transport regime in the films. The electron mobility was found to exhibit in-plane anisotropy with a ratio of  $\sim 1.8$ . Theoretical estimates of the temperature-dependent electron mobility including optical phonon, acoustic deformation potential and remote ionized impurity scattering were found to satisfactorily match the measured data. The synthesis approach reported here demonstrates the feasibility of device quality few-layer MoS<sub>2</sub> films with excellent uniformity and high quality.

Recently, there has been a rapidly increasing interest on investigating layered 2-dimensional (2D) materials such as MoS<sub>2</sub>, WS<sub>2</sub>, WSe<sub>2</sub> *etc.* for their promise towards a variety of next-generation electrical<sup>1,2</sup> and optoelectronic<sup>3,4</sup> device applications including low cost, flexible<sup>5</sup> and transparent electronics.<sup>6,7</sup> From an epitaxial point of view, these materials circumvent limitations associated with lattice mismatch in heterostructure growth of conventional semiconductors and could enable growth of crystalline epi-layers highly lattice mismatched with substrate.<sup>8</sup> Among the 2D materials of the dichalcogenide (MX<sub>2</sub>) family, field effect transistors (FETs) with high on/off ratio and high current densities were fabricated based on MoS<sub>2</sub>,<sup>1,2</sup> MoSe<sub>2</sub>,<sup>9</sup> and WS<sub>2</sub>,<sup>10</sup> while both p-FET and n-FET based on WSe<sub>2</sub>,<sup>11, 12</sup> were also reported besides demonstration of MoS<sub>2</sub>-based simple integrated circuits.<sup>13</sup>

Most of the MoS<sub>2</sub>-based devices reported till date have been fabricated on flakes of MoS<sub>2</sub> mechanically exfoliated from geological samples. These exfoliated micro-flakes of MoS<sub>2</sub> have randomly distributed thickness and orientation, and are not viable for large-scale device integration. To achieve epitaxy of large-area MoS<sub>2</sub> films with uniformity and control, chemical vapor deposition (CVD) methods using various precursors such as MoO<sub>3</sub>,<sup>14-18</sup> MoO<sub>2</sub>,<sup>19</sup> MoCl<sub>5</sub>,<sup>20</sup> Mo<sup>21, 22</sup> and (NH<sub>4</sub>)<sub>2</sub>MoS<sub>4</sub><sup>23, 24</sup> or physical vapor transport method<sup>25</sup> have been employed. However, these large-area films are mostly polycrystalline with small crystal grain sizes from tens of nanometers to several micrometers. In this report, we demonstrate large area vapor-solid-grown epitaxial MoS<sub>2</sub> thin films on sapphire with in-plane and out-of-plane ordering over centimeter length scales. The high quality of these films leads to record high carrier mobility (~200 cm<sup>2</sup>/Vs) for synthetic films at room temperature and current density in excess of 0.15 mA/μm. This work demonstrates the feasibility of device quality few layer MoS<sub>2</sub> layers with sufficient uniformity and quality to enable a variety of device applications based on 2D layered materials.

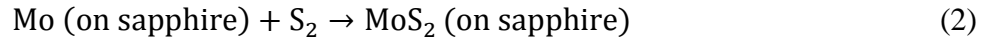
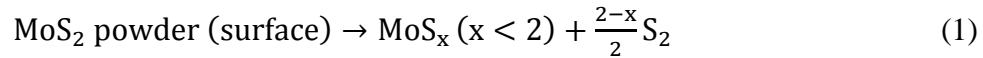
The vapor-solid grown MoS<sub>2</sub> films are of significantly higher crystalline quality than previous attempts.<sup>21</sup> This can be attributed to three main factors - use of epitaxial substrates, control of grain nucleation, and high growth temperatures. We used an epitaxial template (sapphire, space group: R-3c) that shares some symmetry with the MoS<sub>2</sub> (space group: P6<sub>3</sub>/mmc) structure, and is thermally stable up to relatively high temperature. It has been shown previously that under similar conditions, the use of an epitaxial template led to significantly better crystal quality.<sup>16, 24, 26-28</sup> In previous reports of CVD-grown MoS<sub>2</sub>, while out of plane ordering was evident from X-ray diffraction (XRD) measurements in the (0001) direction, no in-plane ordering, such as that evidenced from off-axis geometry, was apparent. We attribute this to significant twist in the mosaic caused by the large number of independent grains.

In this work, the control of grain nucleation was achieved by the supersaturation of sulfur vapor. Single-crystal (0001)-orientated sapphire substrates were solvent cleaned and 5 nm of molybdenum was deposited by sputtering using AJA Orion RF/DC Sputter Deposition Tool. 8.0 mg of MoS<sub>2</sub> powder (purchased from Sigma Aldrich) was placed in a small quartz tube which was then put inside a larger quartz tube (inner diameter: 1 cm) along with the Mo-coated sapphire wafer. The larger quartz tube was pumped down by a mechanical pump, sealed and heated to 1100°C for 4.5 hours and then cooled down to room temperature at a rate of 0.5 °C/min.

Nucleation is the first step in the crystallization process. Nuclei formed in this step can continue to grow into crystalline domains. In order to get single-crystal MoS<sub>2</sub> films with good crystalline nature, the nuclei density should be minimized, which can be achieved by a controlled low supersaturation. In our vapor-solid synthesis, initially sulfur vapor reacts with the surface Mo metal and creates the seed crystal. Sulfur pressure needs to stay at a low value to reduce the nucleation density. It is difficult to control the amount of sulfur by using elemental sulfur itself because the

super saturation is very high compared to the small amount of Mo metal on the substrate. We reduced the sulfur pressure by using MoS<sub>2</sub> powder as a sulfur source to get a low sulfur pressure during the synthesis (Figure 1). Thermogravimetric analysis (TGA) of MoS<sub>2</sub> shows that above 950°C, sulfur can be gradually released and detected by mass spectrometer.<sup>29-32</sup> The decomposition of MoS<sub>2</sub> powder at high temperature can provide sulfur to sulfurize the Mo metal on sapphire substrate. The equilibrium between MoS<sub>2</sub> powder and sulfur vapor inside the quartz tube would provide a sulfur vapor pressure of 0.023Pa at 1100°C.<sup>30</sup> According to the pressure-temperature phase diagram of Mo-S system,<sup>33</sup> this pressure is the lowest sulfur pressure at which pure MoS<sub>2</sub> phase can be produced. The total amount of sulfur that MoS<sub>2</sub> can release under vacuum for 4.5 hours is about 0.099%,<sup>30</sup> which is calculated to be the amount of sulfur that the Mo layer on substrate needed to get MoS<sub>2</sub> phase (calculation result in Supporting Information).

During the synthesis, the following reactions occur:



(0001)-orientated sapphire was chosen to be a good Van der Waals epitaxy substrate due to its atomically flat surface without dangling bonds on the surface. Both theoretical<sup>34, 35</sup> and experimental<sup>36, 37</sup> study show that the surface of (0001)-orientated sapphire is terminated by one Al layer because in this situation the dangling bonds on the surface are either completely filled or empty to form an auto-compensated neutral surface. Thus, the lattice matching condition has been relaxed dramatically.

The surface morphology of the samples was characterized by atomic force microscope (Veeco Instruments DI 3000). Crystalline nature was examined by a Bruker D8 High-Resolution Triple Axis X-Ray Diffractometer. Raman spectra were obtained by Renishaw spectrometer with a 10 mW laser at 514 nm.

Device fabrication started with standard lithography using an i-line stepper projection aligner followed by e-beam evaporation of Ti/Au/Ni metal stack for Ohmic contact. The devices were then mesa isolated using  $\text{BCl}_3/\text{Ar}$  plasma chemistry in an inductively coupled plasma/reactive ion etching (ICP-RIE) system at 30 W RIE power. An Agilent B1500 parameter analyzer was used to measure room temperature current-voltage characteristics on TLM (Transfer Length Method) pads of width 100  $\mu\text{m}$ . Dielectric deposition was done at 250<sup>0</sup>C using a Picosun SUNALE R-150B Atomic Layer Deposition tool. Low temperature I-V measurements were done using a Lake Shore cryogenic set-up equipped with liquid Helium closed-loop circulator.

Figure 2A is an image of as-grown  $\text{MoS}_2$  film with mirror-like appearance due to its atomically smooth surface (rms roughness  $\sim 0.53$  nm, 5  $\mu\text{m}$  x 5  $\mu\text{m}$  atomic force microscopy (AFM) scan, Figure 2B). In fact, the surface of as-grown  $\text{MoS}_2$  sample reported here appeared to be smoother compared to that of 4-5nm  $\text{MoS}_2$  film exfoliated from geological  $\text{MoS}_2$ .<sup>38</sup> The thickness of the  $\text{MoS}_2$  film from sulfurizing 5nm Mo is approximately 7.0 nm based on AFM measurement (Figure 2C). The 2- $\theta/\omega$  XRD scan (Figure 3A) exhibits only the (0001) family diffractions of  $\text{MoS}_2$  and the diffraction of sapphire (0006) peak, which indicates a preferred growth orientation of  $\text{MoS}_2$  with the c-axis parallel to that of sapphire substrate. Thickness fringes near the  $\text{MoS}_2$  (0002) peak suggest a sharp interface (Figure 3A) and confirmed the thickness  $\sim 7$  nm estimated from AFM scan (Supporting Information).

The off-axis (10-13)  $2\text{-}\theta/\omega$  XRD scan (Figure 3B) across the full range of  $\phi=360^\circ$  shows six peaks at  $\text{MoS}_2$ (10-13) position (Figure 3C) due to the six-fold symmetry of the hexagonal phase of  $\text{MoS}_2$  and indicates the single-crystalline nature of as-grown  $\text{MoS}_2$  film. A full range  $\phi=360^\circ$  scan of the sapphire (01-12) substrate taken with the sample in the same position showed three peaks of single-crystalline sapphire corresponding to its three-fold symmetry. The  $\phi$ -scans showed that the unit cell of  $\text{MoS}_2$  was rotated by  $30^\circ$  with respect to that of sapphire substrate. To understand the in-plane orientation between  $\text{MoS}_2$  and sapphire, we show the relative orientations of the two basal planes in Figure 4. The  $\text{MoS}_2$  film and the sapphire substrate are rotationally commensurate: the length of 7  $\text{MoS}_2$  unit cells equals to the length of 8 sapphire unit cells after  $30^\circ$  rotation. The  $30^\circ$  rotation between the epi-layer and the substrate reduces the in-plane lattice mismatch to 13.0% with  $\sqrt{3}a(\text{MoS}_2) = 5.47 \text{ \AA}$ ,  $a(\text{sapphire}) = 4.758 \text{ \AA}$ . For the unrotated case, the lattice mismatch of  $\text{MoS}_2$  and sapphire with  $a(\text{MoS}_2) = 3.16 \text{ \AA}$  and  $a(\text{sapphire}) = 4.758 \text{ \AA}$  would have been 50.5%. The lattice mismatch of 13% is still relatively high, but as shown previously,<sup>39</sup> Van der Waals epitaxial materials can tolerate a higher degree of lattice mismatch than that expected in traditional epitaxy.

Triple-axis rocking curve scan was also measured to confirm the single crystalline nature (Figure 3D). A full width at half maximum (FWHM) of 15.552 arc sec at  $\text{MoS}_2$  (0002) diffraction was found to be about one-half of that of exfoliated single-crystalline  $\text{MoS}_2$ .<sup>21</sup> The narrow rocking curve FWHM suggests that the  $\text{MoS}_2$  films grown by vapor-solid method had high crystalline quality with relatively low density of defects. The two characteristic Raman peaks of  $\text{MoS}_2$  were observed with  $E_{2g}^1$  at  $381.2 \text{ cm}^{-1}$  and  $A_{1g}$  at  $406.5 \text{ cm}^{-1}$  with a peak separation of  $25.3 \text{ cm}^{-1}$  confirming the film had the characteristics of bulk (or several-layer)  $\text{MoS}_2$ .<sup>40</sup>

The carrier mobility, which is strongly dependent on the crystalline quality as well as on the background impurity of the 2D film, plays a critical role in transport properties and hence on device performance. Theoretical calculations<sup>41</sup> and experiments<sup>42, 43</sup> show that while charge impurity limited scattering in single-layer MoS<sub>2</sub> is  $\sim 17 \text{ cm}^2\text{V}^{-1}\text{s}^{-1}$  without the high- $\kappa$  dielectric screening effect, the intrinsic phonon-limited mobility of single-layer as well as multilayer MoS<sub>2</sub> is expected to be as high as  $320\text{-}410 \text{ cm}^2\text{V}^{-1}\text{s}^{-1}$ .<sup>44, 45</sup> Without the high- $\kappa$  dielectric, few-layer MoS<sub>2</sub> films have been shown to have mobility from 10 to  $100 \text{ cm}^2\text{V}^{-1}\text{s}^{-1}$ <sup>46-48</sup> which can be enhanced to several hundred  $\text{cm}^2\text{V}^{-1}\text{s}^{-1}$  with a high- $\kappa$  dielectric environment.<sup>46, 47, 49</sup> However, the high mobility values reported were on exfoliated samples, rather than on large area synthetic MoS<sub>2</sub>. In this report, we show that high mobility approaching the phonon-limited values can be achieved using the synthesis method describe here.

In a log-log scale (Figure 5A), the current-voltage (I-V) curves exhibited two distinct slopes with a linear dependence on V at low-bias regime (0-10 V) and a quadratic dependence at higher (>20 V) bias regime. Further, for various TLM (Transfer Length Method) spacing (d), the current at higher bias was found to have  $V^2/d^2$  dependence, indicating space-charge nature of the transport. The I-V curves were thus fitted with the space-charge transport equation:

$$I = \frac{q n \mu t L}{d} V + \frac{2 \epsilon_s \mu L}{\pi d^2} V^2 \quad (3)$$

Here, q: electron charge,  $\mu$ : electron mobility, t: thickness of MoS<sub>2</sub> film (= 7 nm), L: width of TLM pads (=100  $\mu\text{m}$ ), d: TLM pad spacing,  $\epsilon_s$ : dielectric constant of bulk MoS<sub>2</sub> (=7.6).<sup>48, 50</sup> From the resulting fit (Figure 5B), an electron mobility of  $120 (\pm 20) \text{ cm}^2/\text{Vs}$  and a carrier density of  $2 \times 10^{11} \text{ cm}^{-2}$  were extracted. Interestingly, from the I-Vs measured in a direction perpendicular (in-plane)



to the direction of measurement as reported above, an electron mobility of  $65 \text{ cm}^2/\text{Vs}$  and a carrier density of  $2 \times 10^{11} \text{ cm}^{-2}$  were extracted by fitting I-Vs to equation (3).

This observation of anisotropic electron mobility (with a mobility-ratio of  $\sim 1.8$ ) in few-layer  $\text{MoS}_2$  in the two mutually perpendicular directions is in agreement with prior theoretical predictions<sup>51</sup> of anisotropic electron effective mass ( $0.53m_0$  vs  $0.73 m_0$ ) for transport in ( $\Lambda_{\min}$ ) and in ( $\perp \Lambda_{\min}$ ) directions of the crystal.

To reduce the effect of surface-related defects and impurities on the mobility, the films were covered with 20 nm of  $\text{Al}_2\text{O}_3$  by atomic layer deposition (ALD). The ALD  $\text{Al}_2\text{O}_3$  can passivate some of the interface charge leading to less remote impurity scattering. The I-Vs measured at various temperatures between two device pads separated by  $3.5 \mu\text{m}$  are shown in Figure 5C, and displayed typical characteristics of space charge transport. The extracted electron mobility showed weak temperature dependence while the carrier density was found to increase slightly from  $1.3 \times 10^{11} \text{ cm}^{-2}$  at 10 K to  $1.7 \times 10^{11} \text{ cm}^{-2}$  at 290 K. The room temperature electron mobility was found to be  $\sim 192 \text{ cm}^2/\text{Vs}$  with ALD  $\text{Al}_2\text{O}_3$  on  $\text{MoS}_2$ , an improvement from  $120 \text{ cm}^2/\text{Vs}$  which was extracted without dielectric on  $\text{MoS}_2$ .

A simple estimation of the electron mobility in few-layer  $\text{MoS}_2$  was made based on polar optical phonon (POP) scattering,<sup>52</sup> acoustic deformation potential (ADP) scattering<sup>53</sup> and remote ionized impurity scattering in 2-dimensional electron gas,<sup>53</sup> assuming an electron effective mass of  $0.53m_0$ . For remote impurity scattering, we assumed that the remote interface charge density ( $n_{\text{fix}}^{2\text{D}}$ ) is located at the ALD/ $\text{MoS}_2$  interface, and that the 2D carriers are in the middle of the few-layer film. Since the 2D sheet carrier in our  $\text{MoS}_2$  film is non-degenerate ( $2 \times 10^{11} \text{ cm}^{-2}$ ), the carrier conduction does not take place predominantly at the Fermi Level. The scattering time was therefore estimated

at any energy 'E' and weighed with density of states and Fermi-distribution over the entire energy range (details in Supporting Information).

Figure 5D shows the temperature dependent electron mobility calculated using POP, ADP and remote impurity scattering times compared with experimentally extracted mobility from our MoS<sub>2</sub> films. For a fixed remote impurity ( $n_{\text{fix}}^{2\text{D}}$ ) of  $1 \times 10^{11} \text{ cm}^{-2}$ , the theoretically estimated mobility seems to have a close fit to those measured data points, validating our scattering time estimates. The  $n_{\text{fix}}^{2\text{D}} = 1 \times 10^{11} \text{ cm}^{-2}$  which gives a good fit between theory and experiment, is also close to the actual carrier density ( $1.3 \times 10^{11} - 1.7 \times 10^{11} \text{ cm}^{-2}$ ) extracted after ALD layer on MoS<sub>2</sub>.

## Conclusion

In conclusion, we reported the vapor-solid growth of high-quality few-layer MoS<sub>2</sub> films at 1100°C using sulfur vapor obtained by decomposing MoS<sub>2</sub> powder. The as-grown surface was found to be atomically smooth and high resolution XRD scans and Raman spectroscopy indicated excellent out-of-plane ordering and epitaxial registry of the films over centimeter length scales. The film was found to exhibit space-charge transport and an electron mobility of  $192 \text{ cm}^2/\text{Vs}$  was extracted at room temperature. We also demonstrated anisotropic electron mobility (with a mobility ratio of  $\sim 1.8$ ) in measurement directions mutually perpendicular to each other. ALD Al<sub>2</sub>O<sub>3</sub> on MoS<sub>2</sub> was found to enhance the electron mobility which showed very weak temperature dependence from 10 K to 290 K. A simple scattering model based on optical phonon, acoustic phonon and remote impurity scattering was found to exhibit a good match with the experimentally extracted mobility. This demonstration of record high electron mobility for synthetic large area few-layer MoS<sub>2</sub> films

is highly promising for enabling a wide variety of large-scale electronic device fabrication based on layered 2D materials.

## **ACKNOWLEDGMENT**

L.M. and Y.W. acknowledge the support from NSF (CAREER, DMR-0955471). D.N, E.L., C.H. Lee and S.R. acknowledge funding from the NSF NSEC (CANPD) Program (EEC0914790) and NSF Grant ECCS-0925529. Y.W. and S.R. acknowledge discussions with Professor James Speck (UC Santa Barbara) on the use of MoS<sub>2</sub> as a sulfur source.

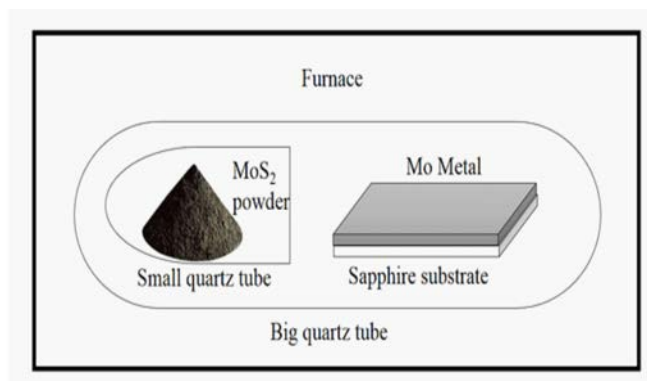


**Figure 1.** The schematic picture of growth set-up.

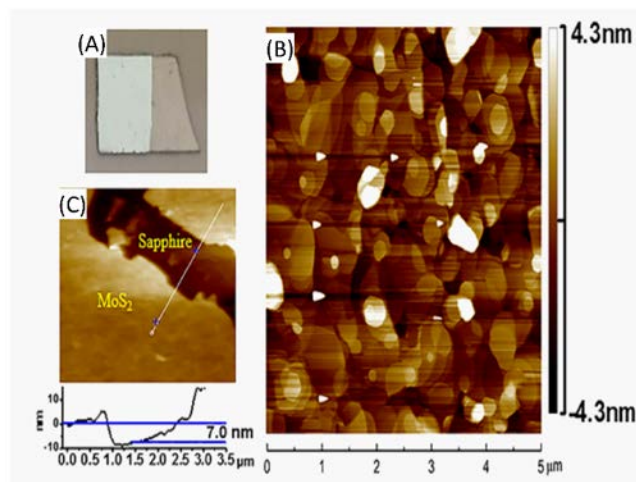


**Figure 2.** (A) Digital image of MoS<sub>2</sub> film; (B) AFM image of MoS<sub>2</sub> film; and (C) AFM images of MoS<sub>2</sub> near the edge to measure the thickness.

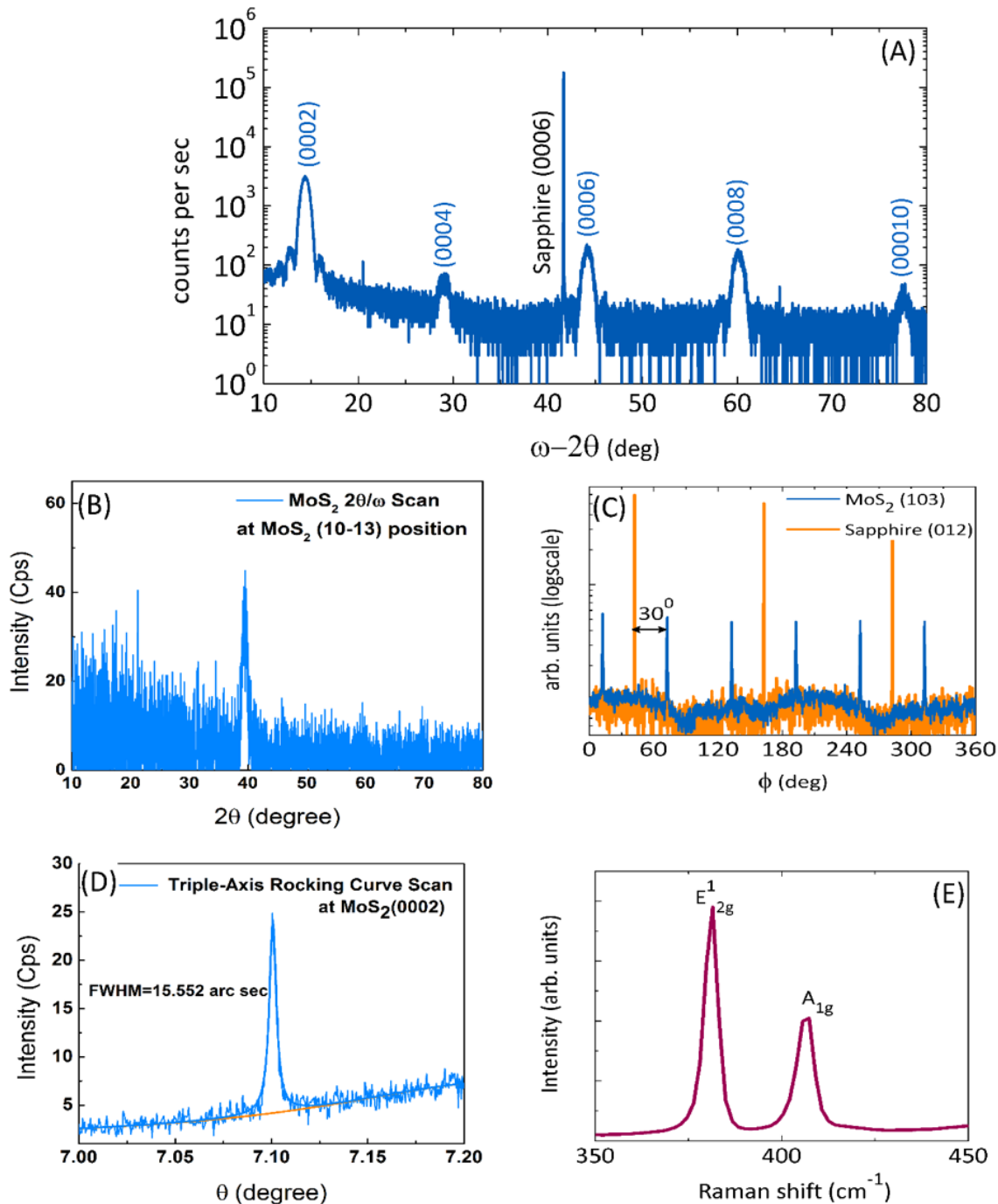


**Figure 3.** (A) 2Theta/Omega XRD Scan of MoS<sub>2</sub> film on sapphire (blue index: MoS<sub>2</sub> diffraction peaks, black index: sapphire (0006) diffraction peak.); (B) 2Theta/Omega XRD Scan at MoS<sub>2</sub> (10-13) position; (C) Phi Scan at MoS<sub>2</sub> (10-13) diffraction position and sapphire (01-12) position; (D)

Triple-Axis Rocking Curve Scan at MoS<sub>2</sub> (0002) diffraction position; and (E) Raman spectra of MoS<sub>2</sub> film.

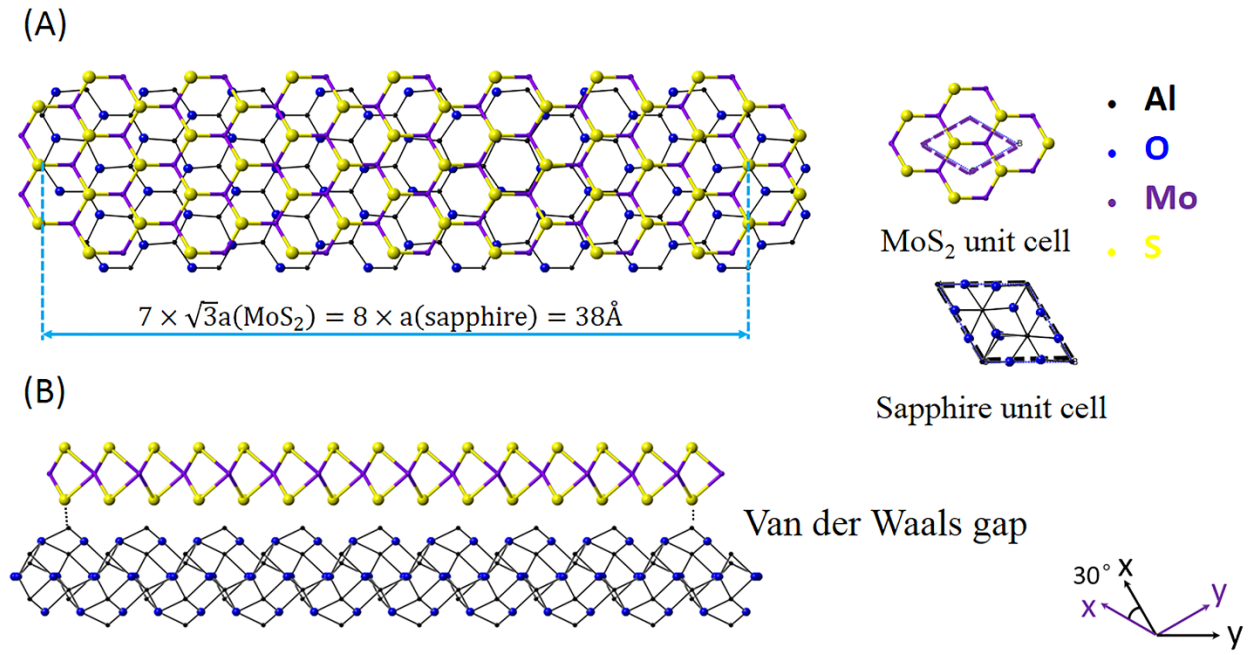


**Figure 4.** Relative in-plane orientation of MoS<sub>2</sub> to sapphire substrate with MoS<sub>2</sub> axis 30° with respect to sapphire: (A) top view and (B) side view. (Black-aluminum atom, blue-oxygen atom, purple-molybdenum atom, yellow-sulfur atom; purple dashed line-unit cell of MoS<sub>2</sub>, black dashed line-unit cell of sapphire).



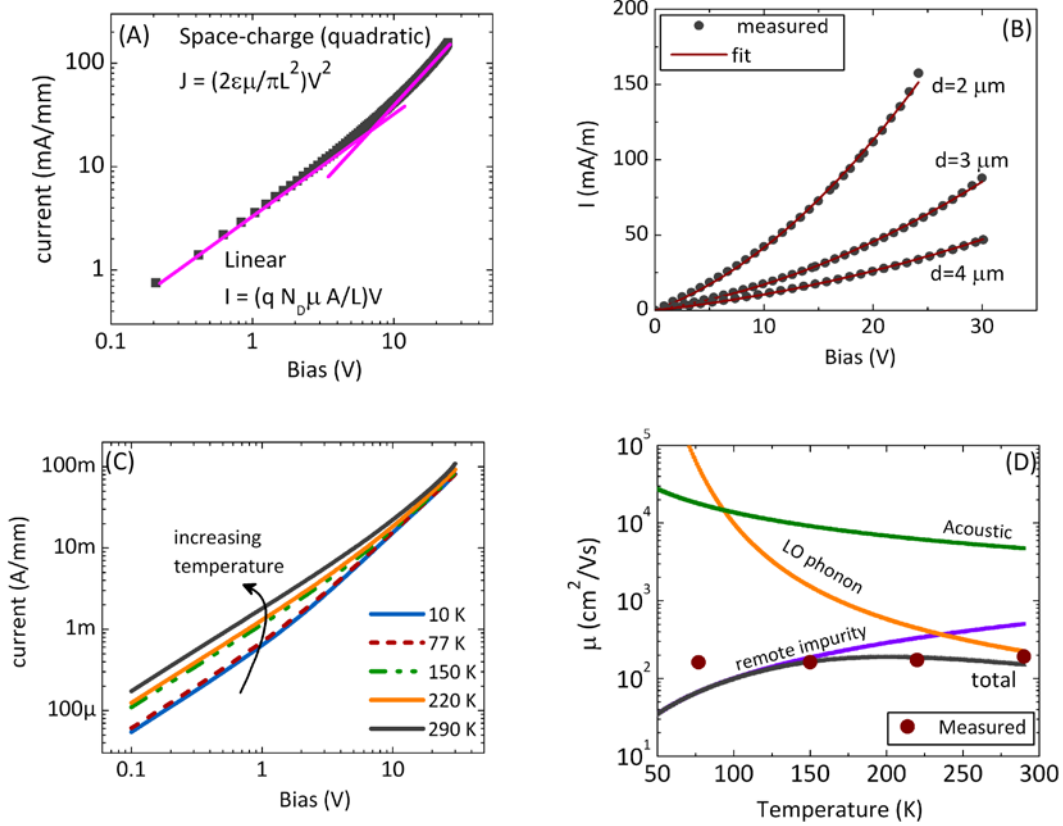


**Figure 5** (A) I-V log-log scale, showing two distinct slopes for linear and quadratic dependence on bias, (B) I-V measured at room temperature for various TLM spacing, along with the fit to  $I = BV + CV^2$ .; (C) Temperature dependent I-V for pad spacing of  $3.5 \mu\text{m}$ ; (D) Theoretical estimates of temperature dependent electron mobility limited by POP, ADP and remote impurity scattering compared with experimentally extracted mobility.

## REFERENCES

1. B. Radisavljevic, A. Radenovic, J. Brivio, V. Giacometti, A. Kis, *Nat Nanotechnol* **2011**, *6*, 147-150.
2. B. Radisavljevic, M. B. Whitwick, A. Kis, *Acs Nano* **2011**, *5*, 9934-9938.
3. R. S. Sundaram, M. Engel, A. Lombardo, R. Krupke, A. C. Ferrari, P. Avouris, M. Steiner *Nano Lett* **2013**, *13*, 1416-1421.
4. W. Choi, M. Y. Cho, A. Konar, J. H. Lee, G. B. Cha, S. C. Hong, S. Kim, J. Kim, D. Jena, J. Joo, *et al. Adv Mater* **2012**, *24*, 5832-5836.
5. H. Y. Chang, S. X. Yang, J. H. Lee, L. Tao, S. W. Hwang, D. Jena, N. S. Lu, D. Akinwande, *Acs Nano* **2013**, *7*, 5446-5452.
6. T. Georgiou, R. Jalil, B. D. Belle, L. Britnell, R. V. Gorbachev, S. V. Morozov, Y. J. Kim, A. Gholinia, S. J. Haigh, O. Makarovskiy, *et al. Nat Nanotechnol* **2013**, *8*, 100-103.
7. G. H. Lee, Y. J. Yu, X. Cui, N. Petrone, C. H. Lee, M. S. Choi, D. Y. Lee, C. Lee, W. J. Yoo, K. Watanabe, *et al. Acs Nano* **2013**, *7*, 7931-7936.
8. A. Koma, *J Cryst Growth* **1999**, *201*, 236-241.
9. S. Larentis, B. Fallahazad, E. Tutuc, *Appl Phys Lett* **2012**, *101*.
10. W. S. Hwang, M. Remskar, R. S. Yan, V. Protasenko, K. Tahy, S. D. Chae, P. Zhao, A. Konar, H. L. Xing, A. Seabaugh, *et al. Appl Phys Lett* **2012**, *101*.
11. H. Fang, S. Chuang, T. C. Chang, K. Takei, T. Takahashi, A. Javey, *Nano Lett* **2012**, *12*, 3788-3792.
12. W. Liu, J. H. Kang, D. Sarkar, Y. Khatami, D. Jena, K. Banerjee, *Nano Lett* **2013**, *13*, 1983-1990.
13. H. Wang, L. L. Yu, Y. H. Lee, Y. M. Shi, A. Hsu, M. L. Chin, L. J. Li, M. Dubey, J. Kong, T. Palacios, *Nano Lett* **2012**, *12*, 4674-4680.
14. Y. H. Lee, X. Q. Zhang, W. J. Zhang, M. T. Chang, C. T. Lin, K. D. Chang, Y. C. Yu, J. T. W. Wang, C. S. Chang, L. J. Li, *et al. Adv Mater* **2012**, *24*, 2320-2325.
15. Y. H. Lee, L. L. Yu, H. Wang, W. J. Fang, X. Ling, Y. M. Shi, C. T. Lin, J. K. Huang, M. T. Chang, C. S. Chang, *et al. Nano Lett* **2013**, *13*, 1852-1857.
16. Q. Q. Ji, Y. F. Zhang, T. Gao, Y. Zhang, D. L. Ma, M. X. Liu, Y. B. Chen, X. F. Qiao, P. H. Tan, M. Kan, *et al. Nano Lett* **2013**, *13*, 3870-3877.
17. A. M. van der Zande, P. Y. Huang, D. A. Chenet, T. C. Berkelbach, Y. M. You, G. H. Lee, T. F. Heinz, D. R. Reichman, D. A. Muller, J. C. Hone, *Nat Mater* **2013**, *12*, 554-561.
18. S. Najmaei, Z. Liu, W. Zhou, X. L. Zou, G. Shi, S. D. Lei, B. I. Yakobson, J. C. Idrobo, P. M. Ajayan, J. Lou, *Nat Mater* **2013**, *12*, 754-759.
19. X. S. Wang, H. B. Feng, Y. M. Wu, L. Y. Jiao, *J Am Chem Soc* **2013**, *135*, 5304-5307.
20. Y. F. Yu, C. Li, Y. Liu, L. Q. Su, Y. Zhang, L. Y. Cao, *Sci Rep-Uk* **2013**, *3*.
21. M. R. Laskar, L. Ma, S. Kannappan, P. Sung Park, S. Krishnamoorthy, D. N. Nath, W. Lu, Y. Wu, S. Rajan, *Appl Phys Lett* **2013**, *102*.
22. Y. J. Zhan, Z. Liu, S. Najmaei, P. M. Ajayan, J. Lou, *Small* **2012**, *8*, 966-971.
23. K. K. Liu, W. J. Zhang, Y. H. Lee, Y. C. Lin, M. T. Chang, C. Su, C. S. Chang, H. Li, Y. M. Shi, H. Zhang, *et al., Nano Lett* **2012**, *12*, 1538-1544.
24. Y. M. Shi, W. Zhou, A. Y. Lu, W. J. Fang, Y. H. Lee, A. L. Hsu, S. M. Kim, K. K. Kim, H. Y. Yang, L. J. Li, *et al. Nano Lett* **2012**, *12*, 2784-2791.
25. S. F. Wu, C. M. Huang, G. Aivazian, J. S. Ross, D. H. Cobden, X. D. Xu, *Acs Nano* **2013**, *7*, 2768-2772.

26. A.Koma, K. Yoshimura, *Surf Sci* **1986**, *174*, 556-560.
27. K. Ueno, K.Saiki,T. Shimada, A. Koma, *Journal of Vacuum Science & Technology a-Vacuum Surfaces and Films* **1990**, *8*, 68-72.
28. F. S. Ohuchi, T. Shimada, B. A. Parkinson, K.Ueno, A. Koma, *J Cryst Growth* **1991**, *111*, 1033-1037.
29. W. A. Brainard, W. A. *The thermal stability and friction of the disulfides, diselenides, and ditellurides of molybdenum and tungsten in vacuum* (10. National Aeronautics and Space Administration ;: Washington, D.C. :, 1968.
30. R. R. Johnston, A. J. W. Moore, *J Phys Chem-Us* **1964**, *68*, 3399-&.
31. G. Jakovidis, K. S. Lemon, A. Singh, E. Taheri, *Commad 2000 Proceedings* **2000**, 316-319.
32. E. Gourmelon, O. Lignier, H. Hadouda, G. Couturier, J. C. Bernede, J.Tedd, J.Pouzet, J. Salardenne, *Sol Energ Mat Sol C* **1997**, *46*, 115-121.
33. Y.Levinsky. *Pressure Dependent Phase Diagrams of Binary Alloys*. Asm International Technical & Engineering Book Service: 1997; p 1838.
34. J. Guo, D. E. Ellis, D. J. Lam, *Phys Rev B* **1992**, *45*, 3204-3214.
35. E. A. Soares, M. A. Van Hove, C. F. Walters,K. F. McCarty, *Phys Rev B* **2002**, *65*.
36. J. Ahn, J. W. Rabalais, *Surf Sci* **1997**, *388*, 121-131.
37. P. Guenard, G. Renaud, A. Barbier, M. Gautier-Soyer, *Surf Rev Lett* **1998**, *5*, 321-324.
38. Y. C. Du, H. Liu, A. T. Neal, M. W. Si, P. D. Ye, *IEEE Elect. Dev. Lett.*, **2013**, *34*, 1328-1330.
39. A. Koma, *Thin Solid Films* **1992**, *216*, 72-76.
40. C. Lee, H. Yan, L. E. Brus,T. F. Heinz, J. Hone, S. Ryu, *Acs Nano* **2010**, *4*, 2695-2700.
41. Z. Y. Ong, M. V. Fischetti, *Phys Rev B* **2013**, *88*.
42. B. Radisavljevic, A. Kis, *Nat Mater* **2013**, *12*, 815-820.
43. B. W. Baugher, H. O. Churchill, Y. Yang, P. Jarillo-Herrero, *Nano Lett* **2013**, *13*, 4212-6.
44. R. Fivaz, E. Mooser, *Phys Rev* **1967**, *163*, 743-&.
45. K. Kaasbjerg, K. S. Thygesen, K. W. Jacobsen, *Phys Rev B* **2012**, *85*.
46. S. Das, H. Y. Chen, A. V. Penumatcha, J. Appenzeller, *Nano Lett* **2013**, *13*, 100-105.
47. W. Z. Bao, X. H. Cai, D. Kim, K. Sridhara, M. S. Fuhrer, *Appl Phys Lett* **2013**, *102*.
48. S. Kim, A. Konar,W. S. Hwang, J. H. Lee, J. Lee, J. Yang, C. Jung, H.Kim, J. B. Yoo, J. Y.Choi, Y. W. Jin, *et al. Nat Commun* **2012**, *3*.
49. H. Liu, P. D. Ye, *IEEE Elect. Dev. Lett.*, **2012**, *33*, 546-548.
50. R. F. Frindt, A. D. Yoffe, Physical Properties of Layer Structures - Optical Properties and Photoconductivity of Thin Crystals of Molybdenum Disulphide. *Proc R Soc Lon Ser-A* **1963**, *273*, 69.
51. H. Peelaers, C. G. Van de Walle, *Phys Rev B* **2012**, *86*.
52. B. L. Gelmont, M. Shur, M. Stroschio, *J Appl Phys* **1995**, *77*, 657-660.
53. J. H. Davies, *The physics of low-dimensional semiconductors: an introduction*. Cambridge university press: 1998.